PLOS ONE

RESEARCH ARTICLE

Optimization of physical and dielectric properties of Co-doped ZnO nanoparticles for low-frequency devices

Adil Muhammad[1], Muhammad Sajid[2]*, Muhammad Nouman Khan[3]*, Muhammed Sheraz[4], Awais Khalid[5,6], Pervaiz Ahmad[7], Satam Alotibi[6], Hamed M. Al-saidi[8], Nebras Sobahi[9], Md Mottahir Alam[9], Sultan Althahban[10], Ahmad M. Saeedi[11], Hasan B. Albargi[12,13]

1 Department of Physics, Islamic International University, Islamabad, Pakistan, **2** School of Material Science, Beijing Institute of Technology, Beijing, China, **3** School of Optics and Photonics, Beijing Institute of Technology, Beijing, China, **4** Department of Physics, Govt: Post Graduate College Mardan, Mardan, Pakistan, **5** Department of Physics, Hazara University Mansehra, Khyber Pakhtunkhwa, Pakistan, **6** Department of Physics, College of Science and Humanities in Al-Kharj, Prince Sattam bin Abdulaziz University, Al-Kharj, Saudi Arabia, **7** Department of Physics, University of Azad Jammu and Kashmir, Muzaffarabad, Pakistan, **8** Department of Chemistry, University College in Al-Jamoum, Umm Al-Qura University, Makkah, Saudi Arabia, **9** Department of Electrical and Computer Engineering, King Abdulaziz University, Jeddah, Saudi Arabia, **10** Department of Mechanical Engineering, Jazan University, Jazan, Saudi Arabia, **11** Faculty of Applied Science, Department of Physics, Umm AL-Qura University, Makkah, Saudi Arabia, **12** Faculty of Science and Arts, Department of Physics, Najran University, Najran, Kingdom of Saudi Arabia, **13** Promising Centre for Sensors and Electronic Devices (PCSED), Najran University, Najran, Kingdom of Saudi Arabia

* sajid.ktk005@gmail.com (MS); noumankhan@bit.edu.cn (MNK)

Citation: Muhammad A, Sajid M, Khan MN, Sheraz M, Khalid A, Ahmad P, et al. (2023) Optimization of physical and dielectric properties of Co-doped ZnO nanoparticles for low-frequency devices. PLoS ONE 18(11): e0287322. https://doi.org/10.1371/journal.pone.0287322

Editor: A. M. Mansour, National Research Centre, EGYPT

Received: March 3, 2023

Accepted: June 3, 2023

Published: November 22, 2023

Data Availability Statement: All relevant data are within the manuscript.

Funding: The authors would like to thank the Deanship of Scientific Research at Umm Al Qura University for supporting this work by Grant Code: (23UQU4350207DSR003).

Competing interests: The authors have declared that no competing interests exist.

Abstract

In this study, zinc-oxide (ZnO) nanoparticles (NPs) doped with cobalt (Co) were synthesized using a simple coprecipitation technique. The concentration of Co was varied to investigate its effect on the structural, morphological, optical, and dielectric properties of the NPs. X-ray diffraction (XRD) analysis confirmed the hexagonal wurtzite structure of both undoped and Co-doped ZnO-NPs. Scanning electron microscopy (SEM) was used to examine the morphology of the synthesized NPs, while energy-dispersive X-ray spectroscopy (EDX) was used to verify their purity. The band gap of the NPs was evaluated using UV-visible spectroscopy, which revealed a decrease in the energy gap as the concentration of Co2+ increased in the ZnO matrix. The dielectric constants and AC conductivity of the NPs were measured using an LCR meter. The dielectric constant of the Co-doped ZnO-NPs continuously increased from 4.0×10^{-9} to 2.25×10^{-8}, while the dielectric loss decreased from 4.0×10^{-8} to 1.7×10^{-7} as the Co content increased from 0.01 to 0.07%. The a.c. conductivity also increased with increasing applied frequency. The findings suggest that the synthesized Co-doped ZnO-NPs possess enhanced dielectric properties and reduced energy gap, making them promising candidates for low-frequency devices such as UV photodetectors, optoelectronics, and spintronics applications. The use of a cost-effective and scalable synthesis method, coupled with detailed material characterization, makes this work significant in the field of nanomaterials and device engineering.

1 Introduction

Metal oxides are thought to be promising materials because of their unique properties such as quantum size effects, large aspect ratios, chemical and thermal stabilities, and so on [1–4]. Among these, Zinc oxide (ZnO) is the wide band gap (3.37 eV) inorganic compound with large excitation energy (60 m eV) belonging to II-VI group. It is usually found in the following basic crystal structures, i.e., wurtzite, Zinc blend, and rock salt [5]. The hexagonal wurtzite structure of ZnO is stable at room temperature and zinc blend structure can be found in a metastable state. Hetro-epitaxial growth on a cubic symmetric substrate can stabilize the zinc blend structure. The lattice parameters of ZnO's wurtzite structure are a = 3.24 Å and c = 5.20 Å [6,7]. As a result of its appropriate physical and chemical properties, ZnO is well-suited for the design of magnetic, electrical and optical devices such as transistors, ZnO-based LEDs and photosensors; solar cells; optical switches; photocatalysts and piezoelectric transducers [8,9]. Furthermore, ZnO has the potential to be very useful in biomedical applications, antireflection coating, and transparent electrodes in solar cells. Applications are restricted by nanoscale high resistivity and high electron-hole pair recombination rate despite its excellent properties [10,11]. Size, morphology tuning and doping with suitable element like TiO_2, CuO, and SiO_2 are the alternative approaches that make them usual for various applications [12]. Various shapes of ZnO nanostructures such as nanorods, nanoparticles, nanocubes, nanowires and nano flowers are already reported [13]. Transition metals (TM = Co, Mn, Fe, Ni etc.) are the most promising materials used to tune their electrical, optical and magnetic properties [14]. Among them, Co is considered as the most effective element for tailoring the optical and dielectric properties due its compatibility with ZnO at nanoscale [15].

The optical and transport characteristics of semiconductor crystal structures are primarily influenced by intrinsic and fundamental flaws. Due to the larger band gap of ZnO than that of GaN, its optical properties are very interesting to researchers [16]. The energy band gap of the composite is altered depending on the amount of doping when TM (Fe, Co, Ni, Mn, etc.) are doped into ZnO.

The band electrons of transition metal ions and exchange interaction of s-pd between confined d state electrons of ZnO semiconductor could be the reason behind smaller energy band gap. The BM (Bursteion Moss) theory says that electrons from dopant elements can live at the bottom of the conduction band, which could explain why transition metals doped into ZnO made the band gap bigger [17,18]. According to the literature review, there is an increase in the crystallite size of ZnO nanoparticles as the dopant ratio of Co ion in ZnO increases. We can calculate the average size of nanoparticle crystallites using Scherrer's formula and Williamson Hall analysis [19–21]. When the frequency is raised, both pure and Co doped ZnO-NPs have lower dielectric constants and higher a.c. conductivities. On the bases of Maxwell and Weigner modes Koop's theory the frequency is explained in which dielectric constant drops [22]. To synthesize the TM doped ZnO nanoparticles different approaches including evaporation condensation, solgel, hydrothermal, sputtering, and co-precipitation can be used [23–26]. These NPs can then be used in a variety of applications. However, in our study, we used the co-precipitation technique to produce pure and Co-doped ZnO-NPs ($Zn_{1-x}Co_xO$) because it is simple and less expensive than the other methods. It is the ultimate goal of this study to use the co-precipitation technique to prepare controllable preparations of Co^{2+} substitute ZnO-NPs, to better understand how the d block element Co^{2+} can be used to dope ZnO in order to enhance its significant properties for the development of novel applications such as spintronics, solar cells photonic devices and Ultraviolet photo sensers, as well as to provide optimized materials for thermoelectric power generators (TEG).

While several studies have examined the magnetic, biomedical, and photocatalytic properties of Co-doped ZnO nanoparticles, there has been limited research on their dielectric

properties [27,28]. This study focuses on the synthesis of Co-doped ZnO nanoparticles using a simple coprecipitation method with varying Co concentrations, followed by a comprehensive analysis of their structural, optical, and dielectric properties using XRD, UV-visible spectroscopy, FTIR, SEM, and dielectric spectroscopy techniques. The results demonstrate that Co doping significantly affects the dielectric properties of ZnO nanostructures, highlighting the potential of these materials for applications in UV photodetectors, optoelectronics, and spintronics devices. This work presents a novel contribution to the field of nanomaterials by providing a deeper understanding of the dielectric properties of Co-doped ZnO nanoparticles synthesized using a cost-effective and scalable technique.

2 Materials and methods

The analytical grade reagents used as raw materials were procured from Sigma-Aldrich. Without further purification, these chemicals were subsequently employed these reagents were subsequently employed for the synthesis of un-doped and Co-doped ZnO NPs. Nanomaterial was synthesized via a simple chemical process using Zinc acetate dehydrate [Zn $(CH_3COOH)_2.2H_2O$, 99%] as a starting material, Cobalt acetate tetra hydrate [Co $(CH_3COOH)_2.4H_2O$, 99%] as a dopant material, sodium hydroxide (NaOH, 99%) to adjust pH value. While acetic acid (CH3COOH, 99.9%) and distilled water (H_2O) were used as a surfactant and reaction medium respectively.

2.1 Synthesis of ZnO and Co-Doped ZnO-NPs

A required amount of [Co $(CH3COOH)_2.4H2O$] and [Zn $(CH3COOH)_2.2H2O$] was obtained in a typical synthesis by adding the precursors in 100 ml of distilled water with continuous magnetic stirring. NaOH solution was added drop wise to increase its pH value. The reaction was then aged for 1h at 100˚ C and adjust the pH up to 11 under vigorous magnetic stirring. The precipitant was collected at room temperature after the reaction was completed and washed with ethanol and distilled water (1:1) using a centrifuge. Finally, the obtained black powder was dried overnight in an electric oven set to 100˚ C. The dried powder was then annealed at 450˚ C for 3 hours to increase the crystallinity. Similarly, all other samples were prepared using the same procedure but with different Co dopant concentrations. Throughout the preparation of these samples, the following chemical reaction has occurred.

$$(1-x)\ Zn\ (CH_3COOH)_2.2H_2O + x\ Co(CH_3COOH)_2.4H_2OZn_{1-x}Co_xO + 6H_2O + 3CO_2 + 5C \quad (1)$$

2.2. Characterization

X-Ray Diffractometry (XRD) CuKa (Model: JDX-3532, JEOL, Japan) was used for structural investigations of prepared NPs. Scanning Electron Microscope (SEM) (Model JSM6410, JEOL, Japan) was employed to study the morphological aspects of the prepared pure and Co doped ZnO-NPs. Ultraviolet-Visible Spectroscopy (UV-Spectroscopy) by Perkin-Elmer (Lambda 25-UV) and Inductor, Capacitor and resistor meter (LCR-meter) (E4980A) were used to study the optical (band gap) and dielectric properties of the prepared NPs.

3. Results and discussion

3.1. X-Ray Diffractometry (XRD) analysis

The structural behaviour of pure and Co doped ZnO nanoparticles was studied using a series of controlled experiments. The crystallinity of the prepared NPs was examined using XRD. An XRD pattern with the typical hexagonal wurtzite structure of ZnO is shown in Fig 1 (JCPDS card no: 036–141). The bands represent the various well observed peaks associated with (100),

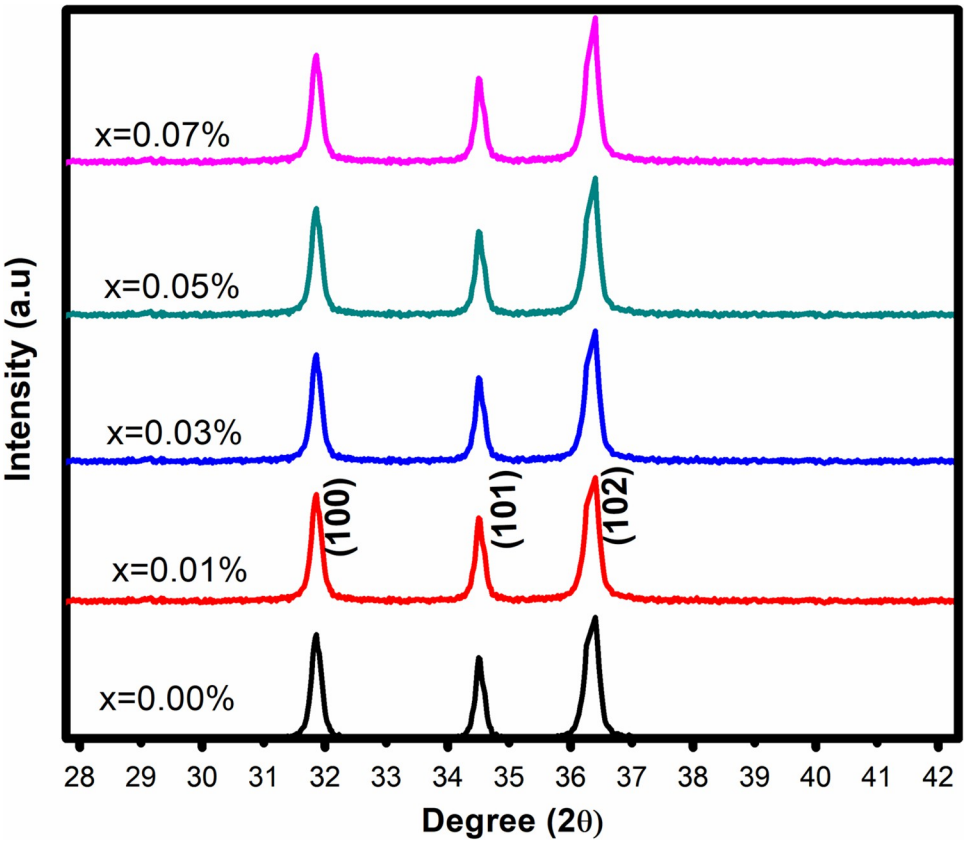

Fig 1. XRD pattern of as synthesized NPs.

https://doi.org/10.1371/journal.pone.0287322.g001

(101), and (102) that agree to wurtzite ZnO at 32˚, 34.5˚, and 36.5˚, respectively. The intensity of the (101) peak increased slightly with increasing Co percentage, indicating an increase in crystallite size and the absence of impure phases of other oxides regardless of dopant concentration.

From the stronger XRD peak, the Scherer's equation is used to determine the crystallite size of all prepared nanoparticles (101).

$$D_{hkl} = \frac{0.9\lambda}{\beta\cos\theta} \tag{2}$$

In which "D" stands for crystallite size, "β" is the entire width at half maximum of the diffraction peak, " λ " for the incoming X-ray wavelength (Cu k_α = 1.54056 Å), and angle of diffraction is represented by "θ".

In X-ray diffraction (XRD), the lattice parameters of a crystal can be calculated using the Bragg equation:

$$n\lambda = 2d\sin\theta \tag{3}$$

where n is the order of the reflection (usually 1), λ is the wavelength of the X-rays used, d is the spacing between crystal planes, and θ is the Bragg angle (the angle between the incident X-ray beam and the crystal plane that reflects the X-ray beam).

The sharp intense peaks (101) for all dopant concentrations including 0.00%, 0.01%, 0.03%, 0.05%, and 0.07%, which, were used to compute the crystallite size of all produced samples i.e.,

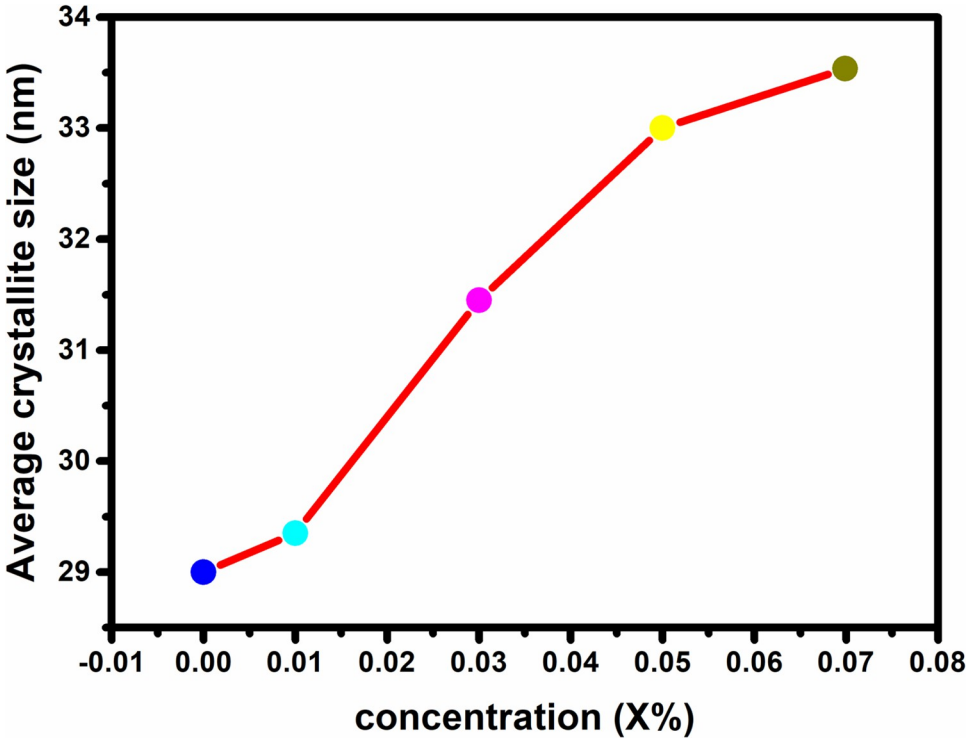

Fig 2. Co dopant Concentration vs. average crystallite size.

https://doi.org/10.1371/journal.pone.0287322.g002

29 nm, 31 nm, 31.45 nm, 33 nm, and 33.5 nm respectively, as shown in Figs 2 and 3 demonstrates that crystallite size grows with increasing Co percentage. The replacement of neighboring Zn with other Co atoms induced lattice assembly distortion due to which rise in crystallite size with increasing Co^{+2} dopant content in ZnO matrix is driven by Co beginning to occupy interstitial locations in addition to substitutional positions. This performance could be attributable to the difference in slit radii between divalent Zn (0.60 Å) and divalent Co (0.58 Å) in tetrahedral coordination. The increase in crystallite size reveals the presence of cobalt in the

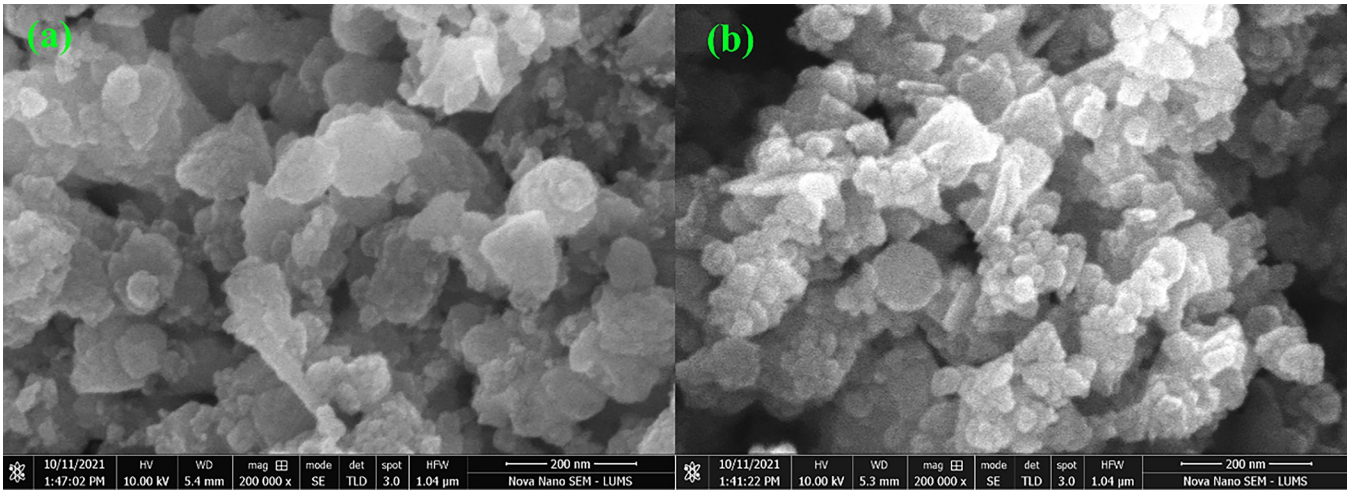

Fig 3. (a) Display a SEM image of pure ZnO-NPs. **(b)** Display a SEM image of 0.05% Co doped ZnO-NPs.

https://doi.org/10.1371/journal.pone.0287322.g003

Table 1. Lattice parameter formula.

Samples	a = b (nm)	C (nm)
ZnO	0.3248	0.5132
$Zn_{0.99}Co_{0.01}O$	0.3248	0.5193
$Zn_{0.97}Co_{0.03}O$	0.3249	0.5196
$Zn_{0.95}Co_{0.05}O$	0.3250	0.5204
$Zn_{0.93}Co_{0.07}O$	0.3252	0.5211

https://doi.org/10.1371/journal.pone.0287322.t001

ZnO lattice. During cobalt doping, distortion is caused by the dopant atoms due to a mismatch between ionic radii of Zn^{2+} and Co^{2+}. This mismatch led to deformation at various points in the ZnO matrix. The increase in deformations results in enhancement in the average crystallite size at higher concentrations of cobalt. As a result, higher cobalt concentrations caused interstitial atoms to be present, which contributed to increase the lattice volume and average crystal size.

The values of lattice parameters a, b and c for pure and Co doped ZnO-NPs are calculated using the formula in Table 1.

3.2 Scanning electron microscopy

Using a SEM, the sample's morphology of the synthesized ZnO and Co doped ZnO-NPs was examined. SEM has opened doors in a variety of disciplines, from engineering to chemistry, giving researchers new and beneficial knowledge about microscopic processes with macroscopic repercussions [29]. Fig 3A and 3B shows SEM images of nanoparticles of pure zinc oxide ($Zn_{1-x}Co_xO$) and nanoparticles with Co^{+2} added ($Zn_{1-x}Co_xO$) with X = 0.00 and 0.05). Pure and Co-doped ZnO ($Zn_{1-x}Co_xO$) are spherical in shape. The average particle size of pure ZnO and Co doped ZnO-NPs is 87 nm and 45 nm which is observed using Image J software, which supports the XRD analysis's assertion even more.

3.3 Energy dispersive X-ray spectroscopy

The EDX spectra of pure zinc oxide nanoparticles (a), Co doped nanoparticles (b), and Co doped nanoparticles (c) with doping values of 0.00 to 0.01 are shown in Fig 4. Nanoparticles of pure zinc oxide (ZnO) show only the zinc (Zn) and oxygen (O) peaks in Fig 4(A). Peaks in the Zn, O, and Co elements are shown in Fig 4(B) and 4(C), with the Co quantity increasing, indicating that Co^{+2} is effectively substituted within the ZnO matrix. No other peaks can be seen other than C (carbon) and Ag (gold) metals that were used in coating to cause scattering back of electrons from the materials during SEM. As expected, the EDX peaks showed that cleaned samples were pure. The percentage of Zn, O and Co different samples are shown in Table 2.

3.4 Energy band gap measurement

Investigating the optical properties of undoped and doped ZnO NPs, as well as other semiconducting NPs, is a common use of UV-visible absorption spectroscopy. By using the Tauc relationship as shown below, the optical band gap of cobalt-doped zinc oxide ($Zn_{1-x}Co_xO$) and pure zinc oxide was measured.

$$(\alpha h\upsilon)^2 = A(h\upsilon - E_g)^n \quad (4)$$

In the above expression, h represents Planck's constant, ν signifies the photon energy, A represents a constant, and the optical band gap is denoted by E_g; "α" represents the absorption

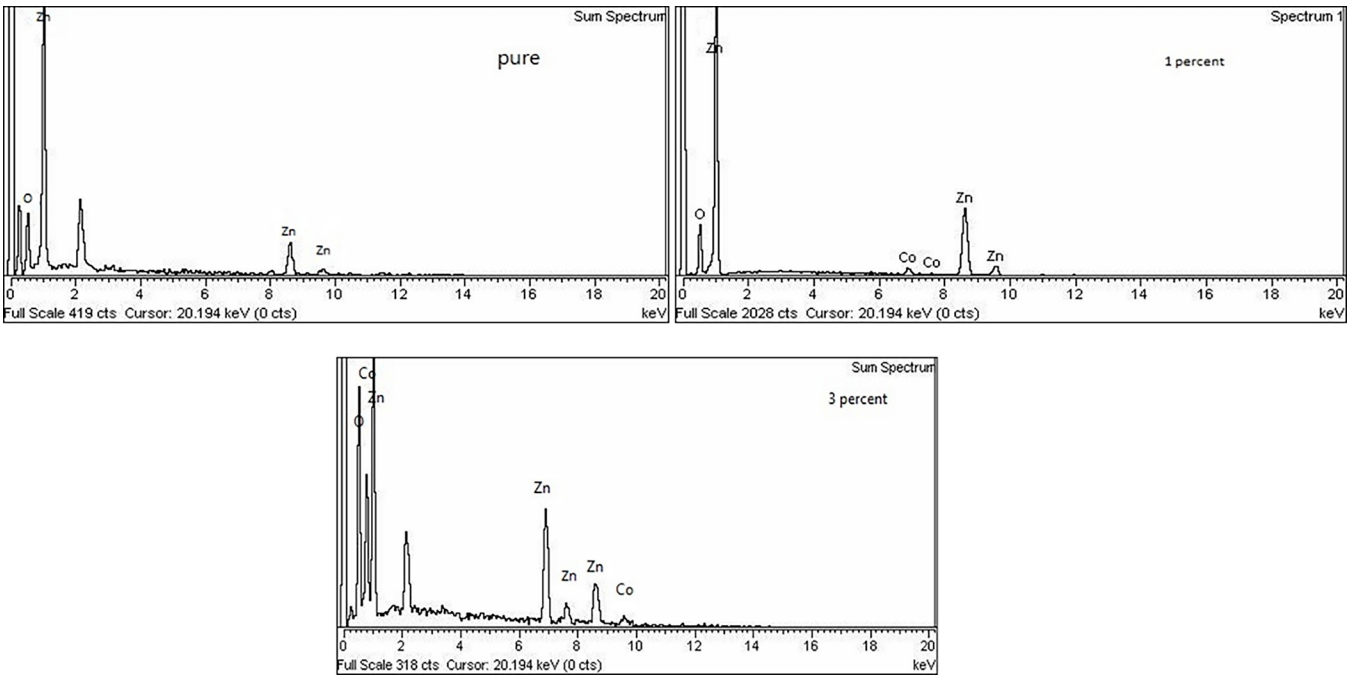

Fig 4. (**a**): EDX spectrum of an undoped sample. (b) Display the EDX spectrum of a $Zn_{0.99}$ $Co_{0.01}$ O sample. (c): Display the EDX spectrum of a $Zn_{0.97}$ $Co_{0.03}$ O sample.

https://doi.org/10.1371/journal.pone.0287322.g004

coefficient ($\alpha = 2.303\frac{A}{t}$) where "A" and "t" represents the absorbance and thickness of the sample. The absorption value of a direct band gap semiconductor is n = $\frac{1}{2}, \frac{3}{2}$, 2 *or* 3, conditional to the electronic transition's nature which were responsible for the absorption. ZnO is a semiconductor with a straight band gap, hence n = $\frac{1}{2}$ is its characteristic value. By plotting $(\alpha h\upsilon)^2$ against photon energy (h), we can calculate the E_g of undoped and varied concentrations of Co doped ZnO NPs, as reported in Fig 5 and Table 3.

It has been discovered that the band gap energy of ZnO reduces as Co^{2+} ion dopant concentration rises. The band electrons of Co^{2+} ions, which replace Zn^{2+} ions and exchange interaction of sp-d between confined "d" electrons may be responsible for potentially lower band gap energy. When doping Co into ZnO nanoparticles, however, Sajid Ali et al. observed an increase in the band gap width with the escalating intensity of doping as shown in Fig 6. It could be due to a drop in the lattice parameter.

3.5 Dielectric properties

These diluted oxides magnetize semiconducting nanoparticles dependent on dielectric properties which were influenced by a variety of factors, including the ratio of Zn^{+2} to Co^{+2} ions,

Table 2. Shows the percentage of Zn, O and Co different samples.

Samples	Zn (W%)	O(W %)	Co (W%)
ZnO	53.87	46.13	0
$Zn_{0.99}Co_{0.01}O$	49.69	49.09	0.22
$Zn_{0.97}Co_{0.03}O$	45.24	50.33	4.43
$Zn_{0.95}Co_{0.05}O$	42.27	51.87	5.86
$Zn_{0.93}Co_{0.07}O$	37.92	54.31	7.77

https://doi.org/10.1371/journal.pone.0287322.t002

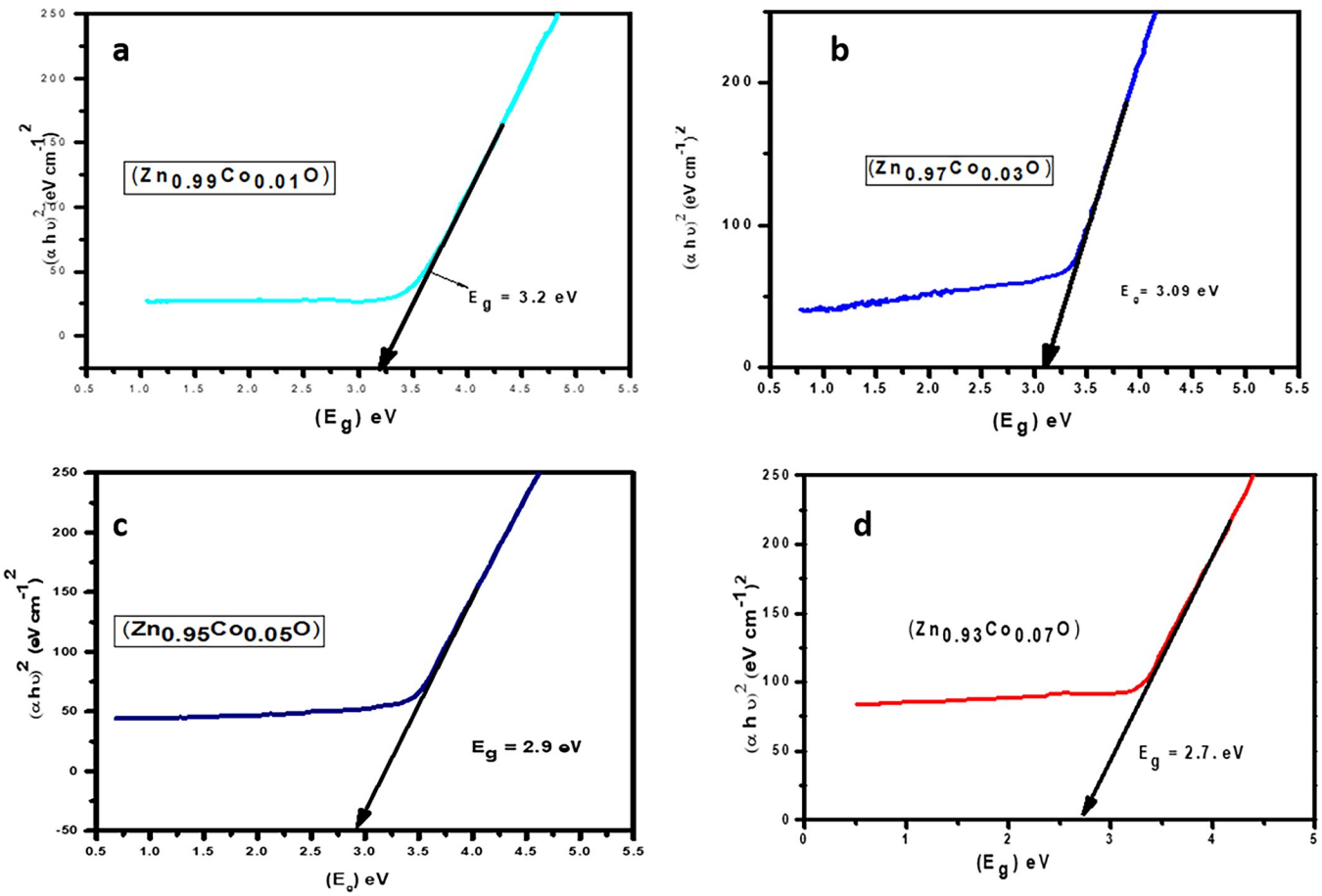

Fig 5. Variation in band gap energy of (a) 0.01%, (b) 0.03%, (c) 0.05%, and (d) 0.07% Co doped ZnO-NPs.

https://doi.org/10.1371/journal.pone.0287322.g005

annealing temperature manufacturing method, chemical composition, and size of particle, and. An important property of Co doped ZnO-NPs is their dielectric properties, which can be used in a variety of applications including optoelectronics, recording media, microwave devices, and transport properties. To investigate the dielectric characteristics, LCR meter has been employed to the synthesized NPs. The sample in a dry powdered form were taken and converted into pallets form before the dielectric measurement. The measurements were carried out in the 1 KHz to 2 MHz frequency range at room temperature in the IIUI's nanoscience lab.

3.5.1 Dielectric constant. The Co_doped ZnO-NPs with varying dopant concentrations are shown in Fig 7 along with their dielectric constant ($\varepsilon^{'}$). Every sample's dielectric constant ($\varepsilon^{'}$) has been found to be maximum at low frequencies, and it exponentially decreases as

Table 3. Energy band gap of various dopant concentration of Co-doped ZnO-NPs.

Samples	Eg (eV)
ZnO	3.4 eV
Zn0.99Co0.01O	3.2 eV
Zn0.97Co0.03O	3.09 eV
Zn0.95Co0.05O	2.9 eV
Zn0.93Co0.07O	2.7 eV

https://doi.org/10.1371/journal.pone.0287322.t003

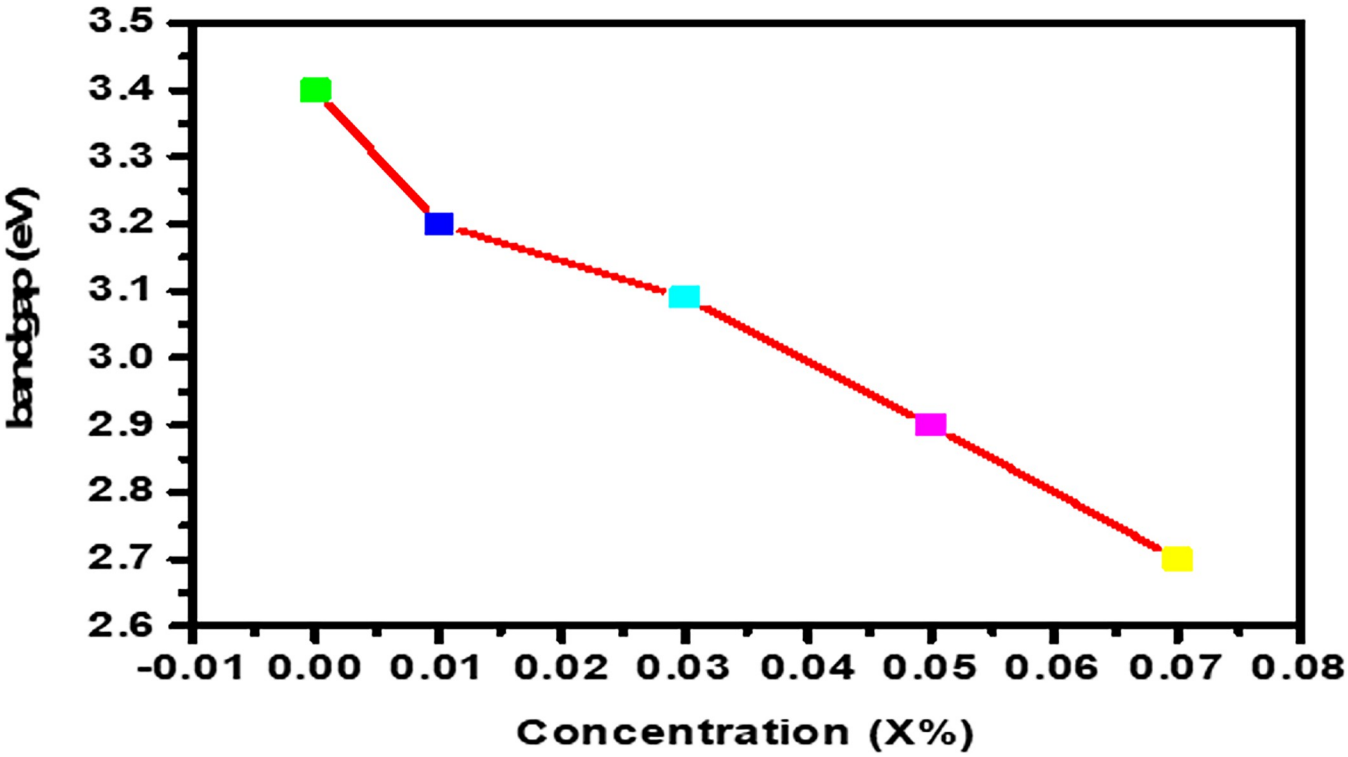

Fig 6. Variation in band gap energy with respect to Co dopant concentration in ZnO-NPs.

https://doi.org/10.1371/journal.pone.0287322.g006

frequency increases. The polarization mechanism with an external field is responsible for this phenomenon. Maxwell-Wagner model and the Koop's phenomenological theory have both been used to explain the dielectric actions of synthesized nanoparticles [30–32].

Koop postulated that crystals have two layers: grains and grain boundaries, with the former serving as a good conductor at low frequencies and the latter being a poor conductor. When these samples are exposed to an external electric field, electrons diffuse to the grain boundaries. Since grain boundaries are very resistive, this causes the electrons to accumulate and produce polarization. This process is known as hooping. At higher frequencies, the dielectric constant drops dramatically as the dipole moment does not coincide with the applied field, and the field has to "duck" to get to the grain boundary electrons [33].

The Maxwell-Wagner model, which has two layers but a uniform medium, is a reference to Koop's phenomenological theory. Since space charge polarization causes a very high gathering of charges at grain boundaries at low frequencies, each sample's dielectric values are very high for this frequency. Every sample's dielectric constant value decrease as the applied electric field frequency increases, but as the frequency increases further, a point is reached where space charge is not involved in the polarization phenomenon, demonstrating that polarization is independent of the applied electric field at high frequencies [34]. The doping level concentration has an impact on the dielectric constant of synthesized nanoparticles as well; for example, in the host material ZnO when doping concentration of Co increases, the dielectric constant (ε') also increases, similarly for each sample. We already know from XRD results that increasing the Co doping level in host ZnO leads to larger crystallites. The dielectric constant (ε') of nanoparticles increases as crystallite size increases [35]. The distortion that occurs at the lattice structure when nearby Zn atoms are replaced by additional Co atoms is what causes the increase in dielectric constant (ε') [36].

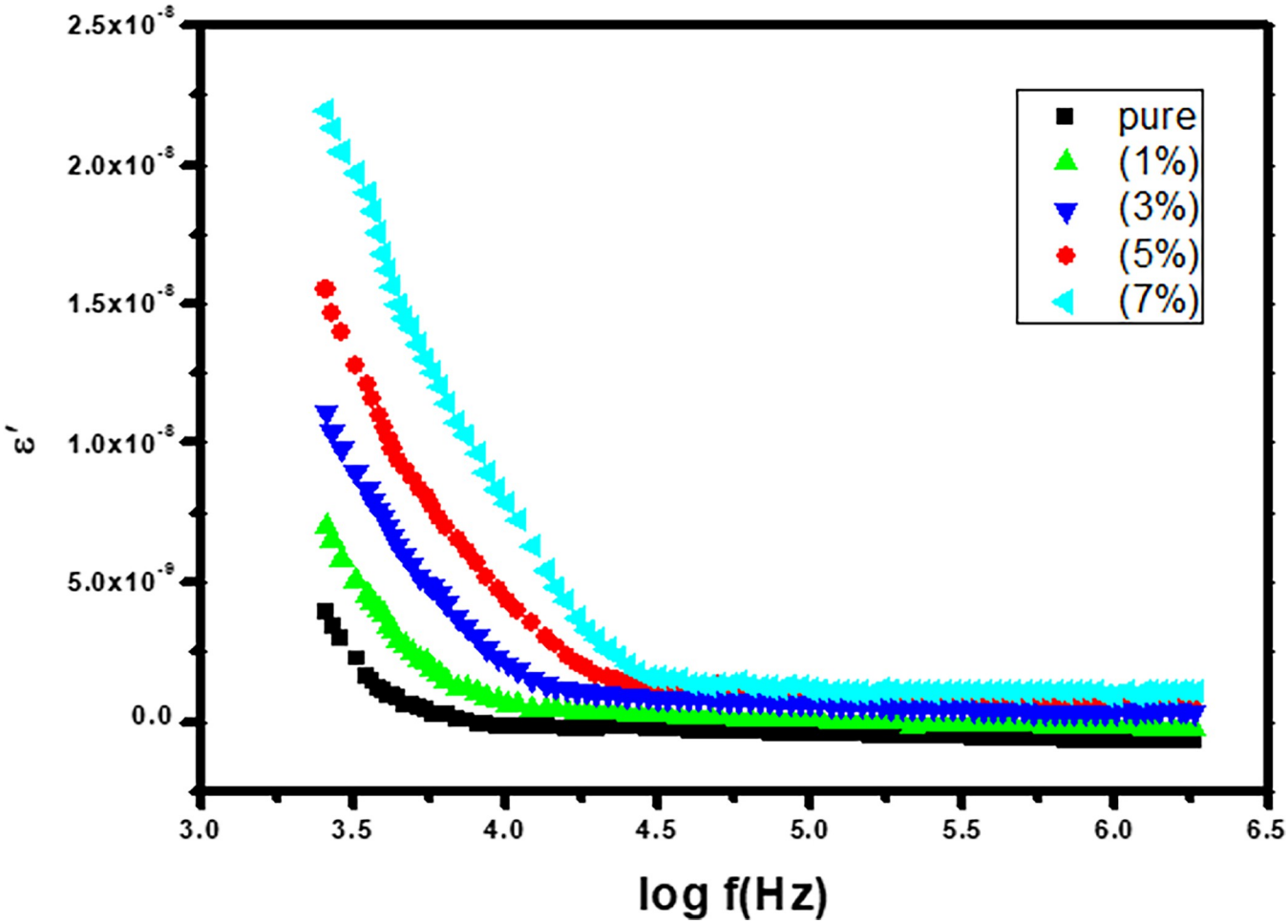

Fig 7. Show real part of dielectric constant with varying frequency.

https://doi.org/10.1371/journal.pone.0287322.g007

3.5.2 Imaginary part of dielectric constant (ε"). The imaginary component of dielectric constant's (ε") is shown in Fig 8 as a function of log frequency for artificial $Zn_{1-x}Co_xO$ nanoparticles with x = 0.00, 0.01, 0.03, 0.05, and 0.07. All synthesized nanoparticles show up on the graph with a large dielectric constant (ε") at low frequencies and vice versa, just as we saw with the real component of dielectric (ε'), something that has been elucidated by the Maxwell Wagner model and Koop's theory. The inset graph in Fig 8 shows how the amount of Co^{2+} doped organized nanoparticles affect the imaginary portion of the dielectric constant (ε"). As the applied frequency is increased, the phenomenon of polarization diminishes, and at higher frequencies, the dipoles exhibit autonomous behavior on the applied frequency, as seen in Fig 8. The inset graph in Fig 8 shows that the imaginary component of the dielectric constant (ε") increases at a similar rate to the increase in Co^{2+} doping content. Since neighboring Zn^{2+} atoms were swapped out for Co^{2+} atoms, the lattice structure has been distorted, leading to a rise in the imaginary portion of the dielectric constant (ε').

3.5.3 AC conductivity. By using the following equation, the ac conductivity of undoped and Co-doped ZnO-NPs has been calculated.

$$\sigma_{ac} = \varepsilon' \varepsilon_{\circ} \omega \tan\delta \quad (5)$$

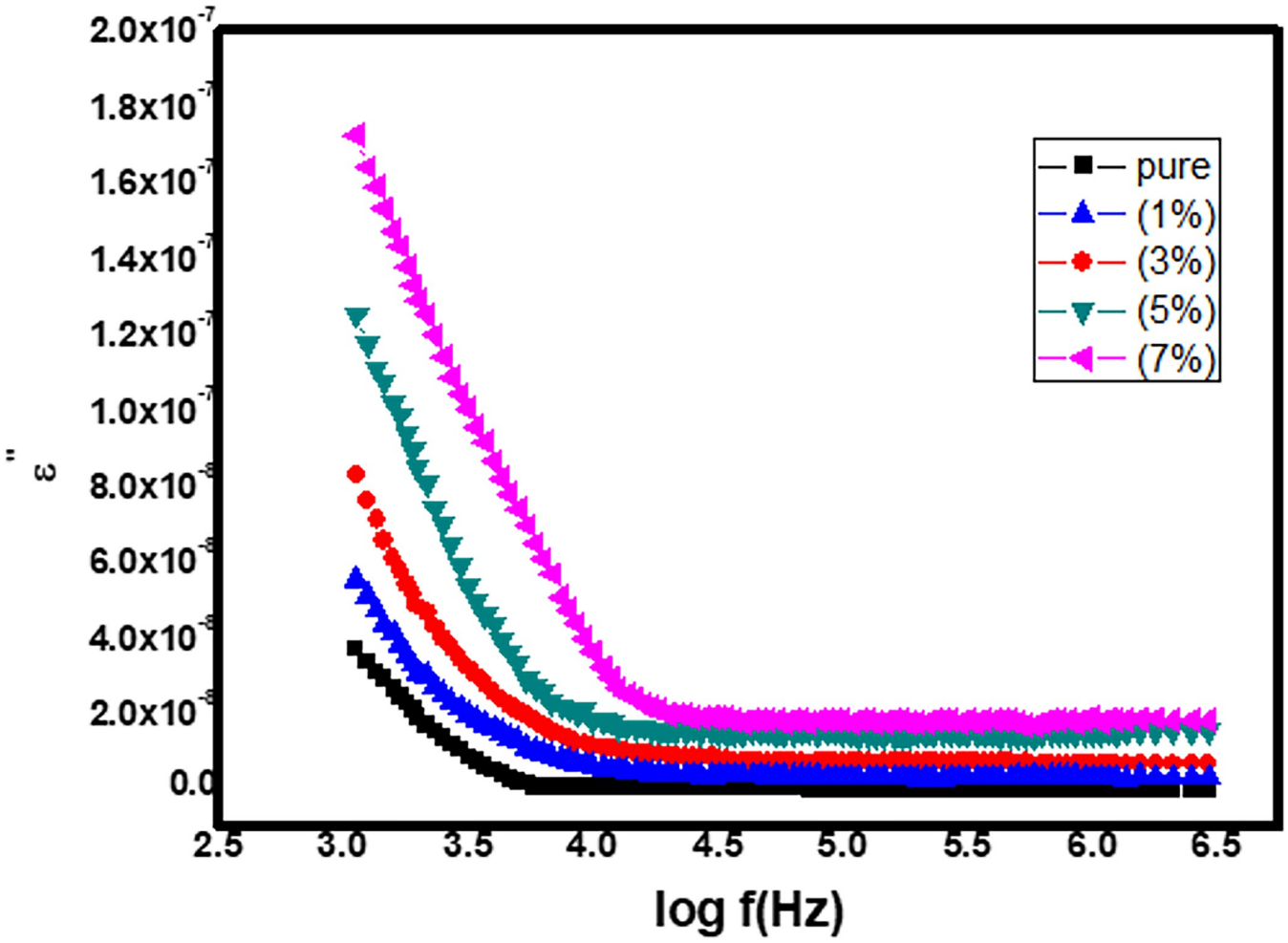

Fig 8. Show imaginary part of dielectric constant with varying frequency.

https://doi.org/10.1371/journal.pone.0287322.g008

The term σ_{ac} in the equation above stands for the a.c conductivity of NPs, ε○ represents the free-space permittivity (8.85×10^{-12} Fm^{-1}), applied field frequency and dispersion factor is denoted by ω and tanδ, $\varepsilon^{'}$ for the real portion of the dielectric. It is clear from Fig 9 that the frequency with which the a.c. conductivity (σ_{ac}) increases. The increment in a.c. conductivity (σ_{ac}) is due to acceleration of the electron hopping process. The graph also shows that a.c conductivity (σ_{ac}) decreases as Co^{2+} dopant content in ZnO increases because Co^{2+} dopant content causes faults in the lattice of ZnO, which may cause the grains to separate at the grain boundaries. As a result, as the level of doping increases, so do the number of faults. This enabled grain boundaries flaw barriers, which in turn caused a roadblock of charge carriers and results in dropping down the a.c conductivity of the sample.

4. Conclusions

Pure and Co-doped ZnO-NPs were prepared using a simple and cost-effective Co-precipitation route. XRD and SEM were used for structural and morphological study. There is no evidence of any additional phases in the X-ray diffraction (XRD) graphs of pure and doped ZnO-NPs with different concentrations of Co (X = 0.00, 0.01, 0.03, 0.05, and 0.07). The average crystallite size, which spans from 29 to 33.5 nm, was calculated using Scherrer's equation. SEM

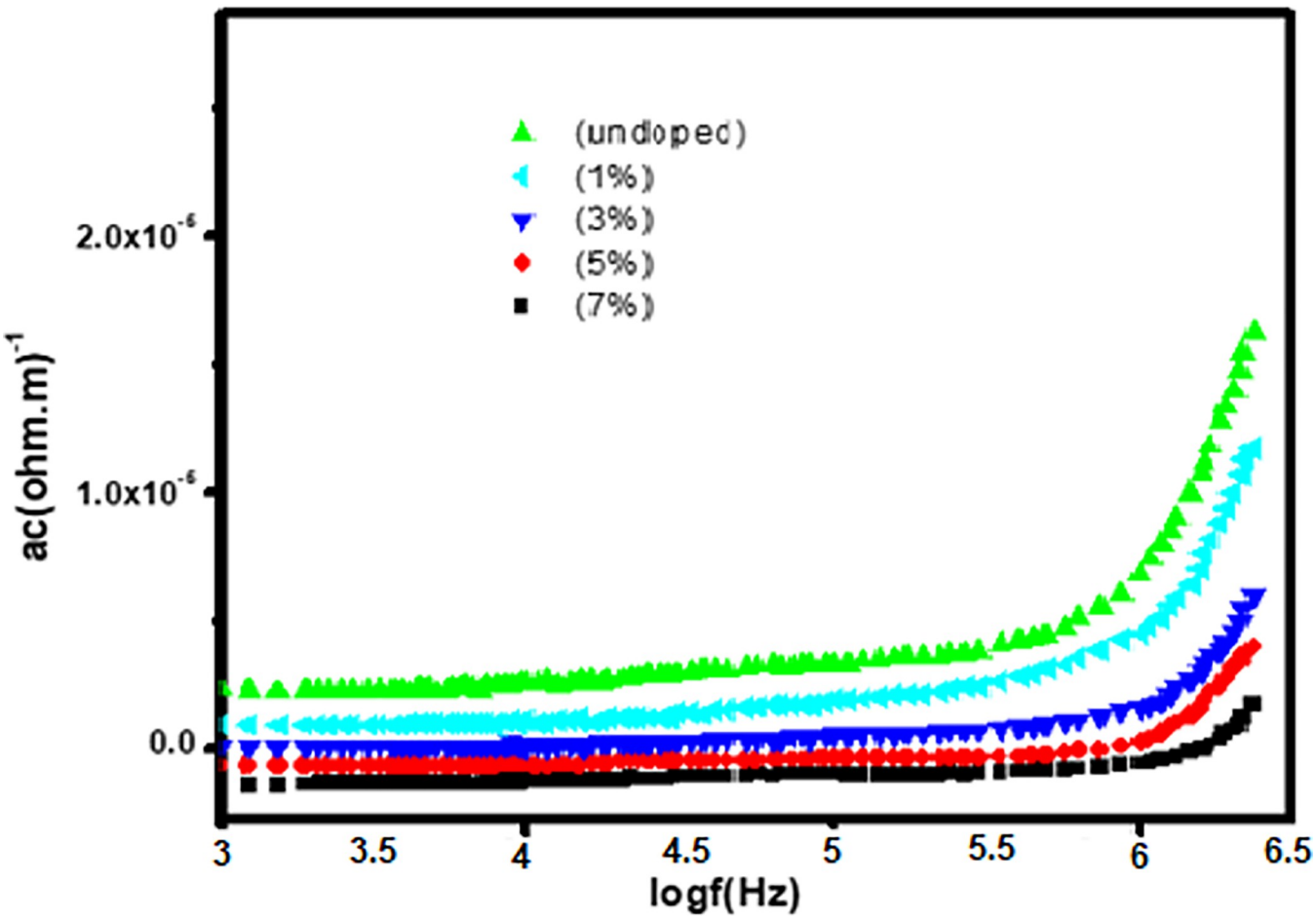

Fig 9. a.c conductivity of pure and Co-doped ZnO ($Zn_{1-x}Co_xO$) nanoparticles.

https://doi.org/10.1371/journal.pone.0287322.g009

micrographs show that pure and Co-doped ZnO ($Zn_{1-x}Co_xO$) are spherical in shape. By using tauc plots the band gap of pure and Co-doped ZnO-NPs was calculated, a reduction in band gap is observed (i.e., 3.4 eV to 2.7 eV) by increasing Co^{2+} ratio in host material. According to the dielectric graphs, the real portion of the ε' and the imaginary part of the ε" are largest at small frequency and nominal at high frequency. The dielectric constant of all Co-doped ZnO-NPs continuously enhanced from 4.0×10^{-9} to 2.25×10^{-8}, and the dielectric loss reduced from 4.0×10^{-8} to 1.7×10^{-7} when Co content increased from 0.01 to 0.07%, whereas a.c. conductivity increases with increasingly applied frequency. Alternating current's conductivity increases exponentially when frequency is applied. Results suggests that Co doping with various concentrations significantly affects the dielectric properties of ZnO-NPs. The prepared particles have a wide and promising applications in UV photodetector, optoelectronic and spintronic.

Author Contributions

Conceptualization: Adil Muhammad, Muhammad Sajid, Muhammad Nouman Khan, Awais Khalid, Pervaiz Ahmad, Satam Alotibi, Hamed M. Al-saidi, Ahmad M. Saeedi, Hasan B. Albargi.

Data curation: Muhammad Sajid, Muhammad Nouman Khan, Ahmad M. Saeedi.

Formal analysis: Adil Muhammad, Muhammad Sajid, Muhammad Nouman Khan, Muhammed Sheraz, Awais Khalid, Satam Alotibi.

Funding acquisition: Awais Khalid, Pervaiz Ahmad, Satam Alotibi, Hamed M. Al-saidi, Ahmad M. Saeedi, Hasan B. Albargi.

Investigation: Adil Muhammad, Muhammad Sajid, Muhammed Sheraz.

Methodology: Muhammad Nouman Khan, Awais Khalid, Pervaiz Ahmad, Hamed M. Al-saidi, Sultan Althahban, Hasan B. Albargi.

Project administration: Satam Alotibi, Nebras Sobahi.

Resources: Awais Khalid, Pervaiz Ahmad, Hamed M. Al-saidi, Md Mottahir Alam, Sultan Althahban, Ahmad M. Saeedi, Hasan B. Albargi.

Software: Muhammed Sheraz, Nebras Sobahi, Sultan Althahban.

Supervision: Pervaiz Ahmad.

Validation: Muhammad Sajid, Satam Alotibi, Hamed M. Al-saidi, Nebras Sobahi, Md Mottahir Alam, Sultan Althahban, Ahmad M. Saeedi, Hasan B. Albargi.

Visualization: Muhammed Sheraz, Pervaiz Ahmad, Nebras Sobahi, Md Mottahir Alam, Sultan Althahban.

Writing – original draft: Adil Muhammad, Muhammad Sajid, Muhammad Nouman Khan, Muhammed Sheraz.

Writing – review & editing: Adil Muhammad, Muhammad Nouman Khan, Awais Khalid, Pervaiz Ahmad, Satam Alotibi, Hamed M. Al-saidi, Nebras Sobahi, Md Mottahir Alam, Sultan Althahban, Ahmad M. Saeedi, Hasan B. Albargi.

References

1. Falcaro P.; Ricco R.; Yazdi A.; Imaz I.; Furukawa S.; Maspoch D.; Ameloot R.; Evans J. D.; Doonan C. J. Application of metal and metal oxide nanoparticles@ MOFs *Coord. Chem. Rev.* 2016, 307, 237–54.
2. Oskam G. Metal oxide nanoparticles: synthesis, characterization and application. *J. sol-gel Sci. Technol.* 2006, 37, 161–4.
3. Dizaj S. M.; Lotfipour F.; Barzegar-Jalali M.; Zarrintan M. H.; Adibkia K. Antimicrobial activity of the metals and metal oxide nanoparticles. *Mater. Sci. Eng. C.* 2014, 44, 278–84. https://doi.org/10.1016/j.msec.2014.08.031 PMID: 25280707
4. Lu J. G.; Chang P.; Fan Z. Quasi-one-dimensional metal oxide materials—Synthesis, properties and applications. *Mater. Sci. Eng. R. Reports.* 2006, 52, 49–91.
5. Raji R.; Gopchandran K. G. ZnO nanostructures with tunable visible luminescence: Effects of kinetics of chemical reduction and annealing. *J. Sci. Adv. Mater. Devices.* 2017, 2, 51–8.
6. Benrezgua E.; Zoukel A.; Deghfel B.; Boukhari A.; Amari R.; Kheawhom S.; Mohamad A. A. A Review on DFT+ U Scheme for Structural, Electronic, Optical and Magnetic Properties of Copper Doped ZnO Wurtzite Structure. *Mater. Today Commun.* 2022, 103306.
7. Hafeez M.; Afyaz S.; Khalid A.; Ahmad P.; Khandaker M.U.; Sahibzada M.U.K.; Ahmad I.; Khan J.; Alhumaydhi F.A.; Emran T.B.; Idris A. M. Synthesis of cobalt and sulphur doped titanium dioxide photocatalysts for environmental applications. Journal of King Saud University-Science. 2022, p.102028.
8. Salehi H.; De, Diego N.; Rad A. C.; Benjamin J. J.; Trevisan M.; Lucini L. Exogenous application of ZnO nanoparticles and ZnSO4 distinctly influence the metabolic response in Phaseolus vulgaris L. *Sci. Total Environ.* 2021, 778, 146331. https://doi.org/10.1016/j.scitotenv.2021.146331 PMID: 33725605
9. Wu W.; Wang Z. L. Piezotronics and piezo-phototronics for adaptive electronics and optoelectronics. *Nat. Rev. Mater.* 2016, 1, 1–17.

10. Sanguramath R. A.; Laadan B.; Raz N.; Katalan A.; Benarroch D. J.; Franco A. CuO (1− x) ZnO x nanocomposite with broad spectrum antibacterial activity: application in medical devices and acrylic paints. *Nanotechnology*. 2021, 32, 215603. https://doi.org/10.1088/1361-6528/abe826 PMID: 33682686

11. Hamrayev H.; Shameli K. Biopolymer-Based Green Synthesis of Zinc Oxide (Zno) Nanoparticles. *IOP Conference Series*: *Materials Science and Engineering*. 2021, vol 1051 (IOP Publishing), p 12088.

12. Es-Haghi A.; Taghavizadeh Yazdi M. E.; Sharifalhoseini M.; Baghani M.; Yousefi E.; Rahdar A.; Baino F. Application of response surface methodology for optimizing the therapeutic activity of ZnO nanoparticles biosynthesized from Aspergillus niger. *Biomimetics*. 2021, 6, 34. https://doi.org/10.3390/biomimetics6020034 PMID: 34072135

13. Kumar Y.; Sahai A.; Olive-Méndez S. F.; Goswami N.; Agarwal V. Morphological transformations in cobalt doped zinc oxide nanostructures: Effect of doping concentration. *Ceram. Int*. 2016, 42, 5184–94.

14. Asaithambi S.; Sakthivel P.; Karuppaiah M.; Balamurugan K.; Yuvakkumar R.; Thambidurai M.; Ravi G. Synthesis and characterization of various transition metals doped SnO2@ MoS2 composites for supercapacitor and photocatalytic applications. *J. Alloys Compd*. 2021, 853, 157060.

15. ElFaham M. M.; Mostafa A. M.; Mwafy E. A. The effect of reaction temperature on structural, optical and electrical properties of tunable ZnO nanoparticles synthesized by hydrothermal method. *J. Phys. Chem. Solids*. 2021, 154, 110089.

16. Zeng H.; Duan G.; Li Y.; Yang S.; Xu X.; Cai W. Blue Luminescence of ZnO nanoparticles based on non-equilibrium processes: defect origins and emission controls. *Adv. Funct. Mater*. 2010, 20, 561–72.

17. Gao H.; Lu B.; Liu F.; Liu Y.; Zhao X. Photocatalytical properties and theoretical analysis of N, Cd-codoped TiO2 synthesized by thermal decomposition method. *Int. J. Photoenergy*. 2012, 453018.

18. Strelchuk V.; Kolomys O.; Rarata S.; Lytvyn P.; Khyzhun O.; Chey C. O.; Nur O.; Willander M. Raman submicron spatial mapping of individual Mn-doped ZnO nanorods. *Nanoscale Res. Lett*. 2017, 12, 1–11.

19. Devesa S.; Rooney A. P.; Graça M. P.; Cooper D.; Costa L. C. Williamson-hall analysis in estimation of crystallite size and lattice strain in Bi1. 34Fe0. 66Nb1. 34O6. 35 prepared by the sol-gel method. *Mater. Sci. Eng. B*. 2021, 263, 114830.

20. Mustapha S.; Tijani J. O.; Ndamitso M. M.; Abdulkareem A. S.; Shuaib D. T.; Amigun A. T.; Abubakar H. L. Facile synthesis and characterization of TiO2 nanoparticles: X-ray peak profile analysis using Williamson–Hall and Debye–Scherrer methods. *Int. Nano Lett*. 2021, 11, 241–61.

21. Ansari S. A. Nisar A.; Fatma B.; Khan W.; Naqvi A. H. Investigation on structural, optical and dielectric properties of Co doped ZnO nanoparticles synthesized by gel-combustion route. *Mater. Sci. Eng. B*. 2012, 177, 428–35.

22. Das S.; Das S.; Roychowdhury A.; Das D.; Sutradhar S. Effect of Gd doping concentration and sintering temperature on structural, optical, dielectric and magnetic properties of hydrothermally synthesized ZnO nanostructure. *J. Alloys Compd*. 2017, 708, 231–46.

23. Khalid A.; et al. Synergistic effects of Cu-doped ZnO nanoantibiotic against Gram-positive bacterial strains. PLOS ONE. 2021, 0251082. https://doi.org/10.1371/journal.pone.0251082 PMID: 33989295

24. Khalid A.; et al. Enhanced Optical and Antibacterial Activity of Hydrothermally Synthesized Cobalt-Doped Zinc Oxide Cylindrical Microcrystals. Materials, 2021. 14(12): p. 3223. https://doi.org/10.3390/ma14123223 PMID: 34207950

25. Khalid A.; et al. Synthesis of Boron-Doped Zinc Oxide Nanosheets by Using Phyllanthus Emblica Leaf Extract: A Sustainable Environmental Applications. *Frontiers in Chemistry*. 2022, 10. https://doi.org/10.3389/fchem.2022.930620 PMID: 35903193

26. Khalid A.; et al. Effect of Cu Doping on ZnO Nanoparticles as a Photocatalyst for the Removal of Organic Wastewater. *Bioinorganic Chemistry and Applications*. 2022, 9459886. https://doi.org/10.1155/2022/9459886 PMID: 35873731

27. Ogale S. B. Dilute doping, defects, and ferromagnetism in metal oxide systems. *Adv. Mater*. 2010, 22, 3125–55. https://doi.org/10.1002/adma.200903891 PMID: 20535732

28. AlAbdulaal T. H.; Ganesh V.; AlShadidi M.; Hussien M. S. A.; Bouzidi A.; Algarni H.; Zahran H. Y.; Abdel-Wahab M. S.; Yahia I. S.; Nasr S. The Auto-Combustion Method Synthesized Eu2O3-ZnO Nanostructured Composites for Electronic and Photocatalytic Applications. *Materials (Basel)*. 2022, 15, 3257. https://doi.org/10.3390/ma15093257 PMID: 35591591

29. Sajid M.; Imran M.; Iqbal J. Tailoring structural, surface, optical, and dielectric properties of CuO nanosheets for applications in high-frequency devices. *Appl. Phys. A*. 2018, 124, 1–8.

30. Khalid A. et al., "Biologically Reduced Zinc Oxide Nanosheets Using Phyllanthus emblica Plant Extract for Antibacterial and Dye Degradation Studies," *Journal of Chemistry*. 2023, 3971686, vol. 2023.

31. Abou Hammad A. B., Bakr A. M., Abdel-Aziz M. S., and El Nahrawy A. M. J. J. o. M. S. M. i. E., "Exploring the ferroelectric effect of nanocrystalline strontium zinc titanate/Cu: Raman and antimicrobial activity," *Journal of Materials Science: Materials in Electronics*. 2020. vol. 31, pp. 7850–7861.

32. Abou Hammad A. B., Darwish A. G., and El Nahrawy A. M. J. A. P. A., "Identification of dielectric and magnetic properties of core shell ZnTiO 3/CoFe 2 O 4 nanocomposites," *Applied Physics A*. 2020. vol. 126, pp. 1–12.

33. El Nahrawy A. M., Hammad A. B. A., Youssef A. M., Mansour A., and Othman A. M. J. A. P. A., "Thermal, dielectric and antimicrobial properties of polystyrene-assisted/ITO: Cu nanocomposites," *Applied Physics A*. 2019. vol. 125, pp. 1–9.

34. El Nahrawy A. M. et al., "Optical, functional impact and antimicrobial of chitosan/phosphosilicate/Al 2 O 3 nanosheets," *Journal of Inorganic and Organometallic Polymers and Materials*. 2020 vol. 30, pp. 3084–3094.

35. El Nahrawy A. M., Ali A. I., Mansour A., Abou Hammad A. B., Hemdan B. A., and Kamel S. J. C. P., "Talented Bi0. 5Na0. 25K0. 25TiO3/oxidized cellulose films for optoelectronic and bioburden of pathogenic microbes," *Carbohydrate Polymers*. 2022. vol. 291, p. 119656. https://doi.org/10.1016/j.carbpol.2022.119656 PMID: 35698357

36. Abou Hammad A. B., Mansour A., and El Nahrawy A. M. J. P. S., "Ni2+ doping effect on potassium barium titanate nanoparticles: enhancement optical and dielectric properties," *Physica Scripta*. 2021. vol. 96, no. 12, p. 125821.